11-19-2010

Systematic Approach to Electrostatically Induced 2D Crystallization of Nanoparticles at Liquid Interfaces

Sumit Kewalramani
Brookhaven National Laboratory, Upton, NY

Suntao Wang
Brookhaven National Laboratory, Upton, NY

Yuan Lin
University of South Carolina - Columbia

Huong Giang Nguyen
University of South Carolina - Columbia

Qian Wang
University of South Carolina - Columbia, wang@mail.chem.sc.edu

See next page for additional authors

Publication Info

Published in *Soft Matter*, Volume 7, Issue 3, 2010, pages 939-945.

Systematic approach to electrostatically induced 2D crystallization of nanoparticles at liquid interfaces†

Sumit Kewalramani,‡§[a] Suntao Wang,‡¶[b] Yuan Lin,[c] Huong Giang Nguyen,[c] Qian Wang,[c] Masafumi Fukuto*[a] and Lin Yang*[b]

Received 9th September 2010, Accepted 26th October 2010
DOI: 10.1039/c0sm00956c

We report an experimental demonstration of a strategy for inducing two-dimensional (2D) crystallization of charged nanoparticles on oppositely charged fluid interfaces. This strategy aims to maximize the interfacial adsorption of nanoparticles, and hence their lateral packing density, by utilizing a combination of weakly charged particles and a high surface charge density on the planar interface. In order to test this approach, we investigated the assembly of cowpea mosaic virus (CPMV) on positively charged lipid monolayers at the aqueous solution surface, by means of *in situ* X-ray scattering measurements at the liquid–vapor interface. The assembly was studied as a function of the solution pH, which was used to vary the charge on CPMV, and of the mole fraction of the cationic lipid in the binary lipid monolayer, which set the interface charge density. The 2D crystallization of CPMV occurred in a narrow pH range just above the particle's isoelectric point, where the particle charge was weakly negative, and only when the cationic-lipid fraction in the monolayer exceeded a threshold. The observed 2D crystals exhibited nearly the same packing density as the densest lattice plane within the known 3D crystals of CPMV. The above electrostatic approach of maximizing interfacial adsorption may provide an efficient route to the crystallization of nanoparticles at aqueous interfaces.

Introduction

Developing the ability to create ordered 2D structures of nanoscale objects is important to fields as diverse as magnetic storage media,[1] photonics,[2] nanoelectronics,[3] and structural biology.[4,5] Among the variety of techniques that are being explored, self-assembly methods[6–8] are particularly attractive because of the possibility of achieving ordered arrays over large area with feature sizes comparable to particles' dimensions. In self-assembly, liquid interfaces play an essential role because nanoparticles are often synthesized as colloidal dispersions[6,8] and because the fluid and defect-free nature of liquid surfaces allows the adsorbed nanoparticles to readily attain equilibrium configuration,[9–11] including 2D crystalline order.[12] Moreover, liquid interfaces can promote self-assembly by modifying the electrostatic inter-particle interactions[13] or through capillary forces.[10,14] Despite these advantages, however, the self-assembly at liquid interfaces has yet to emerge as a widely applicable approach to crystallizing nanoparticles. One major obstacle is that understanding the mechanism of interfacial assembly is often complicated by the interplay between interactions of various origins.[15] Another is that the multi-component nature of typical assembly systems makes it difficult to explore the large parameter space and elucidate the underlying phase behavior. These challenges are especially severe for the assemblies that rely on electrostatic interactions at aqueous interfaces, as described further below.

In the present study, we focus on electrostatics-driven assembly of charged nanoparticles on oppositely charged fluid interfaces, which is relevant to a large majority of water-soluble nanoparticles. Previous proof-of-concept studies demonstrated that electrostatic interactions enhanced the adsorption of charged nanoparticles and biological macroions to oppositely charged Langmuir monolayers at the air–water interface.[16] The utility of this approach is exemplified by its successful application to 2D protein crystallization,[4,5,17–19] which provides a route to the structural analysis of proteins that do not crystallize easily in 3D.[4,5] In addition, ordered assemblies have been formed by colloids on oppositely charged fluid-phase vesicles[20] and by plant viruses at a liquid–liquid interface[21] and at aqueous interfaces of substrate-supported lipid monolayers.[22] However, identifying general conditions for 2D crystallization has remained a significant challenge. On one hand, these previous studies suggest that substantial screening of the inter-particle repulsion, as can be achieved by using salts, is conducive to ordered assembly. On the other hand, it was also noted[5] that if the salt content of the solution was too high (>∼100 mM), very little adsorption of nanoparticles occurred because the interface-particle attractions were highly screened. These findings illustrate that the same experimental parameter can act as an inhibitor or promoter of 2D crystallization. Moreover, disparate sets of experimental

[a]*Condensed Matter Physics and Materials Science Department, Brookhaven National Laboratory, Upton, NY, 11973, USA. E-mail: fukuto@bnl.gov*
[b]*National Synchrotron Light Source, Brookhaven National Laboratory, Upton, NY, 11973, USA. E-mail: lyang@bnl.gov*
[c]*Department of Chemistry and Biochemistry and Nanocenter, University of South Carolina, Columbia, SC, 29208, USA*

† Electronic supplementary information (ESI) available: Measurement of isoelectric point of CPMV and the estimated ionic strength of aqueous subphase. See DOI: 10.1039/c0sm00956c

‡ These authors contributed equally to this work.

§ Present address: Department of Materials Science and Engineering, Northwestern University, Evanston, IL, 60208, USA.

¶ Present address: Department of Physics, Cornell University, Ithaca, NY, 14850, USA.

conditions have been used to induce crystallization, such as pH, ionic strength, and the presence of multivalent ions or polymers. Therefore, it is not surprising that a unified mechanism or simple rules for electrostatics-driven 2D crystallization have not been revealed.

Here we demonstrate a strategy for ordered 2D assembly that takes advantage of the behavior of weakly charged nanoparticles near an oppositely charged interface. It is well established that a charged planar surface that is in contact with an aqueous solution is accompanied by the condensation of counterions.[23,24] When a pair of large, oppositely charged surfaces come close to each other in solution, their association is favored because of the entropy gain that results from the release of counterions into the bulk.[23–25] Then, it is reasonable to expect more particles to adsorb to a fluid interface of a given charge density if the charge carried by each particle is less, driven by both the particle's reduced capacity for balancing the interface charge and the weaker electrostatic inter-particle repulsion (Fig. 1A). The same logic implies that for nanoparticles with given charge, the number of particles adsorbing to a planar interface should increase with increasing interface charge density (Fig. 1A). Thus, by reducing the particle charge and/or increasing the interface charge density, it may be possible to induce dense lateral packing and 2D ordering of electrostatically bound nanoparticles. By investigating the assembly of cowpea mosaic virus (CPMV) on cationic lipid monolayers as a function of pH and the interface charge density, we show that 2D crystallization occurs in the region of the experimental parameter space where the electrostatic interactions are expected to maximize the particle adsorption.

CPMV was chosen because of its intrinsic monodispersity and the ability to vary its charge through pH. Specifically, CPMV is an icosahedral plant virus with a spherically averaged outer diameter of 28 nm[26–28] and maintains its structural integrity over a pH range of 3.5–9.0.[11] In aqueous solutions, CPMV is expected to be neutral at the measured isoelectric point of p$I = 4.3 \pm 0.1$ (see ESI, Fig. S1†), positively charged for pH < pI, and negatively charged for pH > pI, with the magnitude of charge increasing with the difference between pH and pI.

The 2D assembly of CPMV was induced by forming a positively charged Langmuir monolayer at the solution–vapor interface (Fig. 1B) that consisted of a mixture of the cationic lipid 1,2-dimyristoyl-3-trimethylammonium-propane (DMTAP) and the neutral lipid 1,2-dimyristoyl-*sn*-glycero-3-phosphocholine (DMPC) in the fluid ("liquid-expanded") phase. This allowed the interface charge density to be easily controlled through the monolayer composition. Specifically, the average molecular area was fixed at $A_{tot}/(N_{PC} + N_{TAP}) = 70$ Å^2 per lipid, where A_{tot} denotes the total surface area, and N_{PC} and N_{TAP} represent the number of DMPC and DMTAP molecules spread on the surface, respectively (see Experimental). The monolayer charge density was given by $+eN_{TAP}/A_{tot} = +ex_{TAP}/(70$ Å$^2)$ with $x_{TAP} = N_{TAP}/(N_{PC} + N_{TAP})$ denoting the mole fraction of DMTAP.

Unlike previous studies on 2D protein crystallization, the present study employed aqueous solutions of relatively low ionic strength (0.1 to 7 mM for 3.5 < pH < 6.5; see ESI, Fig. S2†) with no multivalent ions or polymeric additives. These simplifying conditions were used to isolate the effects of pH-induced variation in the particle charge on the 2D assembly behavior. The structures of the 2D assembly of lipid-bound CPMV were measured by grazing-incidence small-angle X-ray scattering (GISAXS) and X-ray reflectivity (XR).

Results

The most significant result of the present study is the finding that the 2D crystallization of CPMV occurs in a narrow pH region just above the isoelectric point, where CPMV carries a weak negative charge (Fig. S1†), and only above a threshold

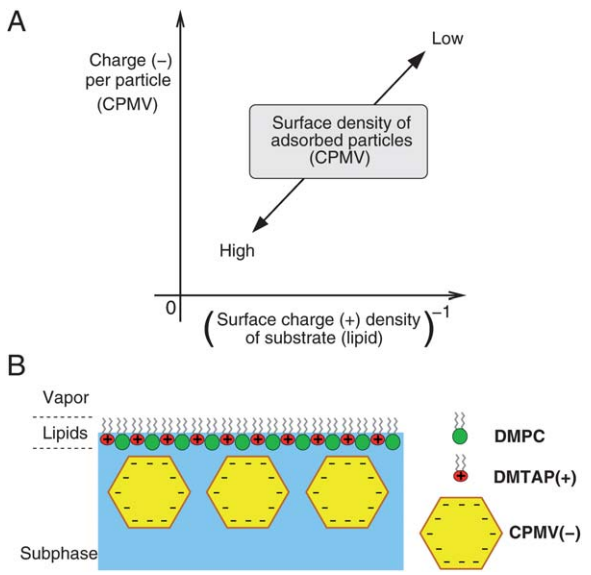

Fig. 1 (A) Expected dependence of the density of adsorbed particles on the particle charge and the inverse surface charge density on the oppositely charged substrate. (B) A schematic illustrating the assembly of cowpea mosaic virus (CPMV) at the lipid-terminated solution–vapor interface.

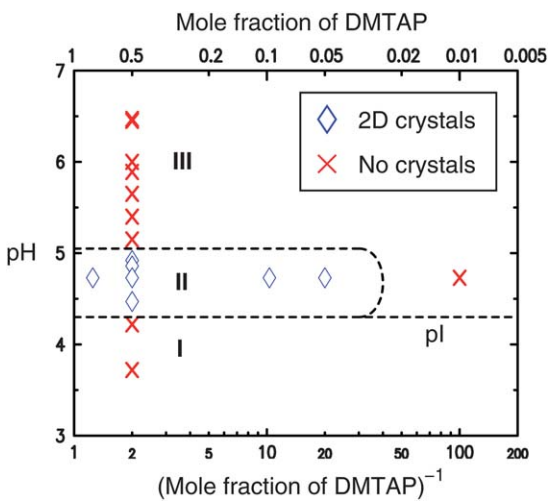

Fig. 2 Observed 2D assembly behavior of CPMV on a cationic lipid monolayer at the aqueous solution–vapor interface, as a function of solution pH and the mole fraction of DMTAP in the binary DMPC/DMTAP monolayer. The points at which grazing-incidence small-angle X-ray scattering (GISAXS) measurements were carried out are indicated by diamonds and crosses, where diamonds represent the observation of GISAXS peaks for the 2D crystals of CPMV.

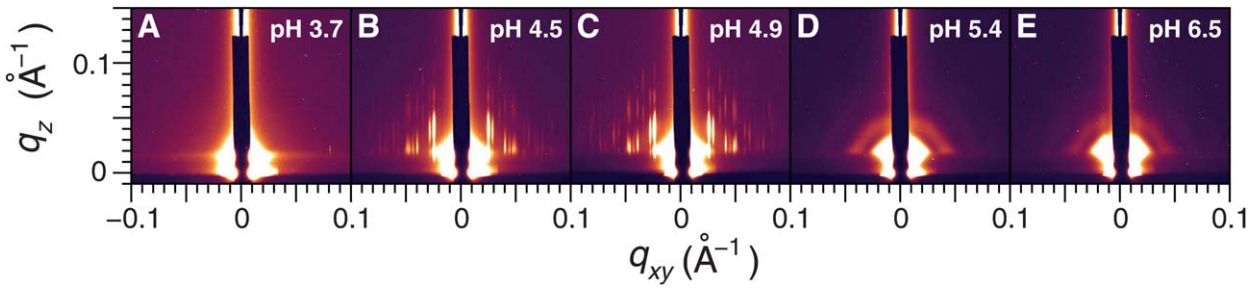

Fig. 3 Measured GISAXS patterns, as a function of the subphase pH, from CPMV assembled on a cationic lipid monolayer (50% DMTAP) at the aqueous solution–vapor interface. (A) For pH below p*I* (~4.3), the data show little evidence for the adsorption of CPMV at the interface. (B and C) For pH just above p*I*, the GISAXS patterns exhibit multiple diffraction peaks from 2D crystals of CPMV. (D and E) For pH well above p*I*, the observed patterns reveal non-crystalline assemblies of CPMV.

monolayer charge density. Fig. 2 summarizes these observations. Fig. 3 shows representative GISAXS data for the pH dependence of CPMV assembly for a lipid monolayer at 50% DMTAP. Distinct assembly behavior is observed in three pH regimes, indicated as I–III in Fig. 2.

In region I (pH < 4.3), the GISAXS patterns show no evidence for the adsorption of CPMV at the interface, exhibiting only the interfacial diffuse scattering along the surface horizon (Fig. 3A). Here, q_{xy} and q_z represent the in-plane and surface-normal components of the scattering vector, respectively.

In region II (4.4 < pH < 5), the GISAXS data reveal the presence of crystalline structure, displaying a series of Bragg rods that are sharply peaked along the q_{xy} axis and highly extended along the q_z axis (Fig. 3B and C). Fig. 4A shows that the positions of the Bragg rods are independent of pH. That these peaks arise from a 2D crystalline monolayer of lipid-bound CPMV is confirmed by a close examination of the Bragg rod intensity profiles and XR measurements, as discussed below. In Fig. 5A, the GISAXS intensity along a Bragg rod from CPMV crystals is plotted as a function of $q = (q_{xy}^2 + q_z^2)^{1/2}$. For comparison, Fig. 5B shows measured small-angle X-ray scattering (SAXS) intensities from bulk solutions of CPMV, which are very similar to the previous SAXS measurements of the CPMV form factor.[27] For both the Bragg-rod profile and the SAXS data at pH 4.0 and 5.5, the separation between the first maximum and the following minimum is $\Delta q \approx 0.017$ Å^{-1}, and that between the first and second maxima is $\Delta q \approx 0.026$ Å^{-1}. This agreement in the modulation periods indicates that the intensity distribution along Bragg rods is modulated by the CPMV form factor. Consequently, the extent to which the CPMV crystals are correlated normal to the interface cannot be larger than the size of the CPMV particle. Further evidence for the monolayer nature of the CPMV crystals is provided in Fig. 6, which shows measured XR data from the lipid-coated surface of a pH 4.7 solution without CPMV (solid lines) and with CPMV (circles). The latter data, corresponding to the interface with CPMV crystals, were collected after an incubation period of over 16 h following the injection of CPMV. The data demonstrate that the adsorption of CPMV causes the XR curve to display additional modulations at low q_z whose period corresponds to an ~300 Å thick layer (Fig. 6B). The agreement between this thickness and the CPMV diameter confirms that only a single layer of CPMV adsorbs at the interface.

In region III (5.1 < pH ≤ 6.5), the GISAXS patterns show no sharp peaks but are instead characterized predominantly by broad, circular ring-like features (Fig. 3D and E), which resemble the intensity envelope for the 2D crystal pattern in region II and the CPMV form factor (Fig. 5B). These observations indicate that for region III, CPMV particles adsorb to the interface, but they form no crystals. However, the existence of a certain degree

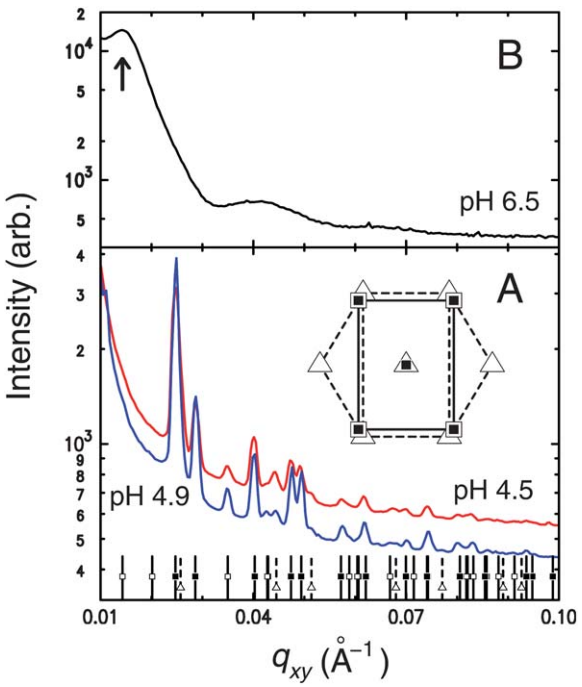

Fig. 4 GISAXS intensities as a function of q_{xy} [integrated over (A) $0.02 < q_z < 0.1$ Å^{-1} and (B) $0.02 < q_z < 0.024$ Å^{-1}], obtained from 2D arrays of CPMV adsorbed on a cationic lipid monolayer (50% DMTAP) at the aqueous solution–vapor interface. (A) 2D crystals at pH 4.5 and 4.9 and (B) non-crystalline arrays at pH 6.5. In (A), the square symbols on the bottom indicate the expected peak positions for the non-centered (open) and centered (filled) rectangular 2D lattice of unit cell dimensions $a_1 = 312$ Å and $a_2 = 439$ Å. The open triangles indicate the expected positions for the hexagonal 2D lattice with the nearest-neighbor distance of $a = 282$ Å. In (B), the upper arrow at $q_{xy} \approx 0.014$ Å^{-1} indicates a peak due to short-range positional correlations between neighboring CPMVs; the broad feature at $q_{xy} \approx 0.04$ Å^{-1} is due to the form factor of CPMV (see Fig. 5B).

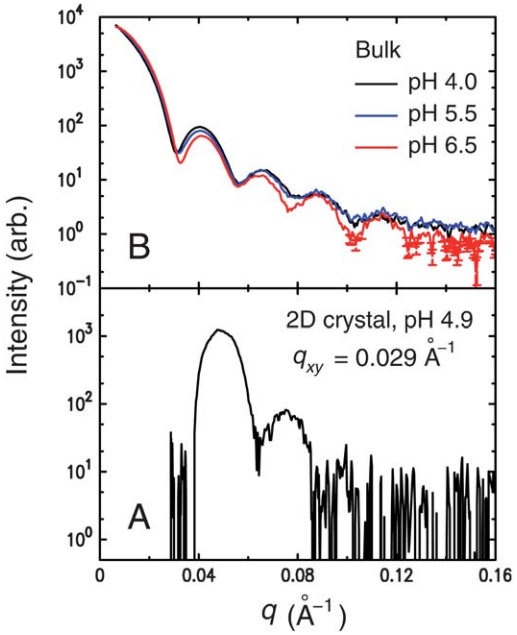

Fig. 5 (A) Background-subtracted GISAXS intensity distribution along a Bragg rod at $q_{xy} = 0.029$ Å^{-1} from CPMV crystals at pH 4.9, where $q = (q_{xy}^2 + q_z^2)^{1/2}$. (B) Measured SAXS data from 10 mM MES solutions of CPMV at pH 4.0, 5.5, and 6.5, whose close agreement supports the integrity of CPMV over the probed pH range. The similarity between the curves in (A) and (B) indicates that aside from a phase shift, the Bragg-rod profile is modulated by the CPMV form factor. The phase shift arises likely because of the interference between the scattering from the vapor interface and the CPMV particle and because of the anisotropic orientation of CPMV in the 2D crystals.

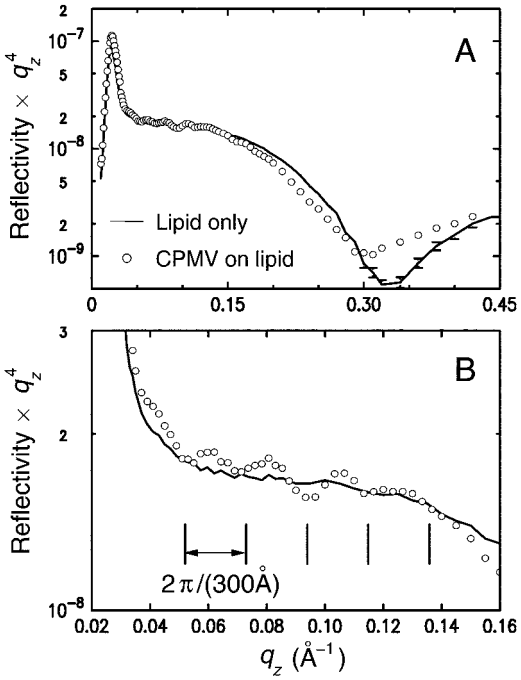

Fig. 6 (A) Measured XR data from a lipid monolayer (50% DMTAP) at the surface of a pH 4.7 solution without CPMV (—) and with CPMV (○). In the presence of CPMV, the XR curve displays additional modulations at low q_z. (B) The vertical bars indicate a modulation period of $\Delta q_z = 2\pi/(300$ Å).

of liquid-like in-plane order[22] is suggested by the observation of a weak q_z-extended peak at small q_{xy}; for example, $q_{xy} \approx 0.014$ Å^{-1} at pH 6.5 (Fig. 3E and 4B). The corresponding spacing $d = 2\pi/q_{xy} \approx 450$ Å is clearly larger than the diameter of CPMV. The broad width (in q_{xy}) of the weak peak and the absence of higher-order peaks at larger q_{xy} are consistent with short-range positional correlations between adsorbed CPMV particles.

Taken together, the above observations show that at 50% DMTAP, 2D crystals of CPMV are formed only in the narrow pH range of 4.4 < pH < 5. The other experimental parameter, *i.e.*, the mole fraction of the cationic lipid DMTAP in the binary lipid monolayer (Fig. 2) scales linearly with the monolayer charge density. Fig. 7 shows in-plane GISAXS intensity profiles from the CPMV assemblies at pH 4.7 as a function of the DMTAP mole fraction. At 1% DMTAP, there is no evidence of CPMV crystallization. By contrast, at or above 5% DMTAP, multiple diffraction peaks are observed indicating that the lipid-bound CPMV have crystallized. The key observation here is that the 2D crystallization of CPMV occurs only above a threshold monolayer charge density.

Within region II (Fig. 2), the positions of the Bragg rods, and hence the lattice parameters for the observed crystals, are independent of pH and the monolayer charge density (Fig. 4A and 7). However, the monolayer charge density affects which crystal forms appear (Fig. 7). Indexing of the observed Bragg peaks (vertical lines and symbols in Fig. 4A and 7) demonstrates that at or above 10% DMTAP, two crystal forms coexist at the interface. The first component, represented by square symbols in Fig. 4A and 7, is a rectangular 2D lattice. The other component, represented by triangles in Fig. 4A and 7, consists of a hexagonal lattice. By contrast, for a monolayer with 5% DMTAP, only hexagonal crystals are observed. We first describe the structural characteristics of the rectangular lattice.

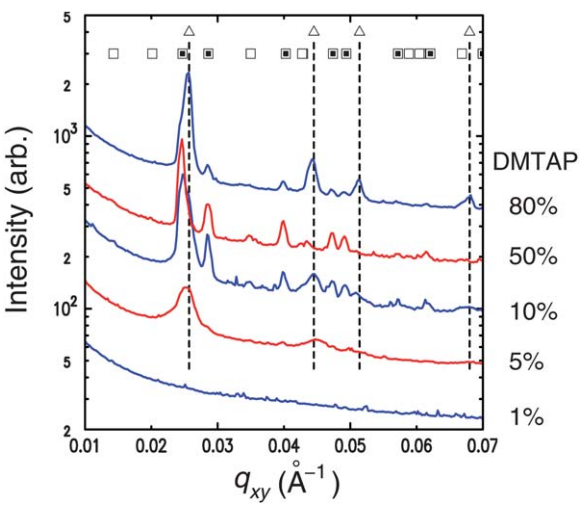

Fig. 7 GISAXS intensities *vs.* q_{xy} (integrated over $0.02 < q_z < 0.07$ Å^{-1}) at various DMTAP mole fractions, obtained from 2D arrays of CPMV adsorbed on cationic lipid monolayers at pH 4.7. The indicated indices are the same as in Fig. 4. The curves are shifted vertically for clarity.

The unit cell dimensions for the rectangular lattice are $a_1 = 312$ Å and $a_2 = 439$ Å. Most of the strong peaks arising from this crystal form can be accounted for by the assumption of a centered rectangular symmetry (filled squares). However, the data display additional weaker peaks (*e.g.*, at $q_{xy} = 0.035$ Å^{-1}) that would be forbidden for the centered rectangular symmetry but are allowed for the non-centered rectangular cell of the same dimensions (open squares). The simplest explanation for the above observation is that the unit cell contains two CPMV particles and that the particle at the center of the unit cell is not strictly equivalent to those at the vertices. The nearest-neighbor (NN) distance of $(a_1^2 + a_2^2)^{1/2}/2 = 269$ Å is slightly smaller than the average spherical diameter of 284 Å for CPMV[27,29] but compares well with the reported outer diameter of 268 Å and 272 Å along the icosahedral particle's threefold axes.[28,30] Clearly, the CPMV particles are oriented anisotropically within the rectangular lattice. The magnitude of the NN distance further suggests that one of the particle's threefold axes points close to the NN direction.

The observed rectangular 2D lattice is very similar to the (110) plane of the body-centered cubic (bcc) lattice (space group $I23$), the denser of the two known 3D crystal forms of CPMV.[28,30] The ratio of the two lattice constants for the rectangular cell ($a_2/a_1 = 1.41$) is equal to $\sqrt{2}$, and the shorter of the two lengths ($a_1 = 312$ Å) agrees well with the cubic lattice parameter of $a = 317$ Å.[28] That the (110) plane represents the plane of highest density for the bcc lattice indicates that the packing in the rectangular 2D crystal is essentially as dense as possible for the CPMV particles.

The hexagonal lattice is characterized by the lattice parameter of $a = 282$ Å. The corresponding packing density [$(\sqrt{3}/2)a^2 = 68\,900$ Å^2 per CPMV] is only slightly smaller, by 0.6%, than that for the rectangular lattice [$(1/2)a_1a_2 = 68\,500$ Å^2 per CPMV]. However, the 2D hexagonal lattice does not correspond to any crystallographic plane of the 3D crystals of CPMV. In the only other known 3D crystal form (the hexagonal space group $P6_122$, $a = 451$ Å, $c = 1038$ Å, 6 particles per unit cell),[29,31] the volume fraction of CPMV is less than 30%, and each particle has only four nearest neighbors. Nevertheless, in this 3D crystal, the particles are separated by an NN distance of 284 Å,[29] as in the case of the hexagonal 2D crystal.

The observed structural characteristics of the two crystal forms suggest that the rectangular crystal is the equilibrium phase and the hexagonal crystal is a precursor or metastable form. This inference is also supported by visual comparison of the intensities of the diffraction peaks from the two lattices, which shows that at 10% and 50% DMTAP, the rectangular form is the dominant component of the two coexisting crystal forms (Fig. 4A and 7). For these reasons, the observation of higher peak intensities for the hexagonal lattice at 80% DMTAP (Fig. 7) is slightly surprising. However, it should be noted that the adsorption rate of CPMV at the interface is expected to increase with the monolayer charge density. If the time scale for adsorption is much smaller than that required for the optimal alignment of particles at the growing crystal front, crystallization into non-equilibrium forms may be observed.[32] Frequently, the non-equilibrium form is a hexagonally packed array.[4] This is likely the reason for the observation of hexagonal lattice as the dominant component at the highest monolayer-charge density.

Discussion

The above 2D assembly behavior of CPMV reflects the pH-dependent variation in the sign and magnitude of the particle's charge and the corresponding change in the role of electrostatic interactions. For region I (Fig. 2), the subphase pH is at or below p*I*, *i.e.*, CPMV is either neutral or positively charged in solution and therefore cannot serve as a macromolecular counterion for the positively charged monolayer. This explains why the interfacial adsorption of CPMV is not observed in region I. On the other hand, for pH > p*I*, CPMV is negatively charged, and the mechanism of counter-ion release[23–25] should promote the adsorption of these particles to the cationic lipid monolayer. This interpretation is supported by the above GISAXS evidence for the presence of interface-bound CPMV in regions II and III.

The lack of long-range order in the 2D assembly in region III can be attributed to predominance of the repulsive electrostatic interactions between the interface-bound particles at high pH. As the solution pH is raised above p*I*, the net negative charge of the CPMV particle is expected to increase. Therefore, the electrostatic inter-particle repulsion should be stronger in region III than in region II. The observation of the relatively large *d*-spacing to diameter ratio in region III ($d/a \approx 1.6$ at pH 6.5) is qualitatively consistent with these expectations. The large d/a ratio and the absence of long-range order likely reflect the long-ranged nature of the repulsive electrostatic interactions in this pH regime. For the subphase solutions used in region III, we estimate the Debye length κ^{-1} to be only a small fraction of the CPMV diameter ($\kappa^{-1}/a \approx 0.40$ at pH 5, ≈ 0.17 at pH 6; see Fig. S2†). Thus, at the observed average spacing of $d \approx 450$ Å, the electrostatic potential between a pair of interface-bound CPMV is expected to be dominated by the slowly varying dipole–dipole repulsion ($\sim 1/d^3$).[10]

The formation of 2D crystals in region II is consistent with the relatively weak net negative charge that CPMV carries in this pH regime. In region II, the number of interface-bound CPMV should be higher than in region III since more particles are needed to balance the positive surface charge on the lipid monolayer. Moreover, the reduced particle charge should diminish the repulsive electrostatic contribution to the overall inter-particle interactions and therefore enhance the relative importance of other contributions, such as the attractive van der Waals interactions. Both these effects should promote dense lateral packing of lipid-bound CPMV. The existence of a mechanism like this for inducing high lateral packing density is evident from the close-packed structures of the 2D crystals that are formed by CPMV.

Our results further demonstrate that the 2D assembly of CPMV can be tuned by varying the mole fraction of the cationic DMTAP in the binary monolayer. In particular, in region II, the 2D crystallization is induced only above a threshold monolayer charge density. Since the adsorption is expected to increase monotonically with the monolayer charge density, the above observation is consistent with the mechanism of density-driven crystallization.

Ordered 2D assemblies of micron- and nano-scale objects have previously been formed at oppositely charged fluid interfaces.[5,17–21] However, the present work is unique for its demonstration of 2D crystallization at low ionic strength (<1 mM for pH 4.4–5.0,

Fig. S2†) and without relying on the use of multivalent ions or polymers. Furthermore, prior to the present study, the electrostatics-driven 2D crystallization has not been systematically examined as a function of the particle charge (*via* pH) or the interfacial charge density. Only in a few instances,[18,33] the interface charge density was varied, but coarsely from zero to arbitrarily chosen finite values. In those studies, because the 2D crystallization of charged particles was observed only on oppositely charged fluid interfaces, it was concluded that attractive electrostatic interactions with the interface drove the adsorption of those particles.

Similarly, the effects of pH on the 2D assembly of nanoparticles have not been carefully studied. A majority of the studies were conducted at pH values where the particles were expected to be highly charged. For example, crystallization of proteins was often induced near physiological conditions (*i.e.*, pH ≈ 6–8), where those proteins were strongly charged.[17–19,33,34] In a recent experiment, the assembly of a plant virus[21] was also studied at a pH value far exceeding the particle's p*I*. The 2D crystallization of these highly charged particles on oppositely charged interfaces was examined only for solutions with high salt concentrations (>∼100 mM) that contained multivalent ions[17–19,21,33,34] and/or polymers.[33] That is, crystallization occurred under conditions where the electrostatic inter-particle repulsion was considerably screened[24] or when the polymers induced inter-particle attraction through depletion forces.[35,36] Despite these trends, however, the difficulties in exploring the vast experimental parameter space have prevented the emergence of general guidelines or simple rules for 2D crystallization.

On the other hand, the 2D crystallization of weakly charged particles (pH ≈ p*I*) was studied only in two isolated instances, ferritin (p*I* = 4.5 ref. 37) at pH ≈ 5.0,[33] and α-actinin (p*I* =6.0) over a pH range of 6.0–8.0.[17] Nevertheless, these studies[17,33] also utilized solutions with high ionic strength (>∼100 mM), which completely obscured the effects of pH or the particle charge. Specifically, no pH dependence could be observed in the crystallization behavior of α-actinin.[17] For these reasons, a direct comparison between these previous studies and the present work is not possible. It is worth noting that in the study of α-actinin,[17] the high density of interface-bound particles required for crystallization was speculated to arise from a highly asymmetric charge distribution on the particle such that the surface apposing the monolayer had a high and opposite charge to that of the monolayer. Such a mechanism is highly unlikely for CPMV, for which an asymmetric charge distribution is implausible because all the 20 triangular faces of the CPMV icosahedron are expected to have the same charge.[26]

Besides the lack of systematic investigation into the effects of key parameters, these previous studies, especially those on protein crystallization, were primarily focused on obtaining high-quality 2D crystals for structural analysis and not on understanding the mechanisms by which electrostatics controlled the adsorption and ordered assembly. Therefore, even in the studies where the experimental phase space was explored, the effects of the parameters were discussed in terms of the crystal sizes and the resolution to which the crystals diffracted.[4,5]

In contrast to these studies, we have demonstrated a simple and rational approach that promotes the 2D crystallization of charged nanoparticles by maximizing the particle adsorption at the oppositely charged interface. These conditions are achieved when the solution pH is very close to (but not equal to) the particle's p*I*, *i.e.*, when the particle charge is weak, and only when the interface charge density is sufficiently high. A practical implication of these results is that the number of iterations or screening experiments required for the 2D crystallization of interface-bound nanoparticles can be significantly reduced. Similar experimental guidelines for crystallization conditions for proteins or colloidal particles in bulk solutions have been known for some time. It has been observed that protein crystallization in 3D typically occurs when the second virial coefficient lies in a very narrow region of weakly negative values.[38–40] At low salt concentrations and in the absence of multivalent ions and polymers, these conditions are met when the particle is weakly charged.[39,40] To the best of our knowledge, no such prediction rules for 2D crystallization of interface-bound nanoparticles were known prior to the present study. A worthy extension of the current work would be to test the generality of the strategy outlined here by studying the assembly of charged inorganic or biological nano-objects at oppositely charged fluid interfaces.

Experimental

Wild-type CPMV was generated as reported previously.[41,42] The lipids DMPC and DMTAP were purchased from Avanti Polar Lipids, Inc. All other chemicals were purchased from Sigma-Aldrich. Aqueous solutions were prepared using ultrapure water (Millipore; 18 MΩ cm).

All the experiments were performed at 23 °C, using the previously described sample cells and preparation procedures.[43] The aqueous subphase contained 10 mM 2-(*N*-morpholino)ethanesulfonic acid (MES) and its pH was adjusted with NaOH or HCl. The estimated ionic strengths (see ESI†) and the corresponding Debye lengths are plotted as a function of pH in Fig. S2†. An appropriate volume of a chloroform solution that contained the two lipids at known concentrations was spread at the interface to form a monolayer at a fixed molecular area of 70 Å^2 per lipid. Within 20 minutes the surface pressure stabilized in the range of 6–12 mN m^{-1}, consistent with the fluid-phase monolayer of double-tail lipids.[44] After the monolayer equilibrated, a solution of CPMV was injected into the subphase through the injection port to achieve a final CPMV concentration of 0.015 mg ml^{-1}. The samples were allowed to equilibrate for at least 15 h prior to X-ray measurements.

X-Ray experiments were performed at Beamlines X9, X21 (GISAXS), and X22B (XR) of the National Synchrotron Light Source, using set-ups and data collection procedures similar to those described previously.[43] The X-ray wavelengths used were λ = 0.855 Å (X9), 1.239 Å (X21), and 1.517 Å (X22B). For GISAXS, a microfocusing mirror was used to set the incident angle to $\alpha \approx 0.7\alpha_c$, where α_c is the critical angle for the air–water interface (α_c = 0.12° at λ = 1.239 Å and α_c = 0.085° at λ = 0.855 Å). The beam size at the sample was 0.4 mm (H) × 0.025 mm (V), corresponding to an illuminated footprint area of ∼0.4 mm × 14 mm. For each sample, the reported GISAXS pattern was obtained by summing the individual images recorded from 14–18 fresh spots on the surface, with a separation of 1 mm between adjacent spots.

Conclusion

We have demonstrated a rational approach for electrostatically inducing the 2D crystallization of water-soluble nanoparticles by studying the assembly of CPMV on a positively charged lipid monolayer at the aqueous solution–vapor interface. In particular, the particle-interface and inter-particle electrostatic interactions were varied systematically through the monolayer charge density (*via* cationic lipid fraction) and the particle charge (*via* pH), respectively. In order to highlight the effects of these two parameters on 2D crystallization, the assembly was carried out at a relatively low ionic strength and without the help of multivalent ions or polymeric additives, in sharp contrast to typical methods used to crystallize colloids and proteins. Significantly, *in situ* X-ray scattering measurements reveal that the 2D crystallization of CPMV on the cationic monolayer is achieved only above a threshold monolayer charge density and only in a narrow pH range where the charge on CPMV is weakly negative. That is, 2D crystals form only in the region of the parameter space where the electrostatic interactions maximize the adsorption of CPMV at the interface. Moreover, the indexing of X-ray diffraction peaks indicates that CPMV particles in the observed 2D crystals are as densely packed as in the (110) plane of the body-centered cubic crystal of CPMV in 3D, *i.e.*, the densest lattice plane known for CPMV. The results support that the assembly of weakly charged particles on a highly and oppositely charged aqueous interface is conducive to density-driven 2D crystallization of water-soluble nanoparticles.

Acknowledgements

We thank H. Hlaing for assistance with sample preparation. The BNL contribution to this work, including use of the National Synchrotron Light Source, was supported by the US Department of Energy, Office of Basic Energy Sciences, Division of Materials Sciences and Engineering, under contract no. DE-AC02-98CH10886. QW acknowledges the financial support from National Science Foundation under contract no. CHE-0748690, Department of Defense under contract no. WN11NF-09-1-236, Department of Energy, Office of Basic Energy Sciences, under contract no. DE-SC0001477, and the W. M. Keck Foundation.

References

1 C. A. Ross, *Annu. Rev. Mater. Res.*, 2001, **31**, 203–235.
2 J. D. Joannopoulos, P. R. Villeneuve and S. H. Fan, *Nature*, 1997, **386**, 143–149.
3 G. Schmid, M. Baumle, M. Geerkens, I. Helm, C. Osemann and T. Sawitowski, *Chem. Soc. Rev.*, 1999, **28**, 179–185.
4 R. D. Kornberg and S. A. Darst, *Curr. Opin. Struct. Biol.*, 1991, **1**, 642–646.
5 J. Dietrich and C. Venien-Bryan, *Strategies for Two-Dimensional Crystallization of Proteins using Lipid Monolayers*, Imperial College Press, London, 2005.
6 S. Kinge, M. Crego-Calama and D. N. Reinhoudt, *ChemPhysChem*, 2008, **9**, 20–42.
7 J. Dutta and H. Hofmann, in *Encyclopedia of Nanoscience and Nanotechnology*, American Scientific Publishers, Valencia, CA, 2004, vol. 9, pp. 617–640.
8 A. N. Shipway, E. Katz and I. Wilner, *ChemPhysChem*, 2000, **1**, 18–52.
9 Y. Lin, H. Skaff, T. Emrick, A. D. Dinsmore and T. P. Russell, *Science*, 2003, **299**, 226–229.
10 F. Bresme and M. Oettel, *J. Phys.: Condens. Matter*, 2007, **19**, 413101.
11 J. T. Russell, Y. Lin, A. Boker, L. Su, P. Carl, H. Zettl, J. B. He, K. Sill, R. Tangirala, T. Emrick, K. Littrell, P. Thiyagarajan, D. Cookson, A. Fery, Q. Wang and T. P. Russell, *Angew. Chem., Int. Ed.*, 2005, **44**, 2420–2426.
12 Z. Jiang, X.-M. Lin, M. Sprung, S. Narayanan and J. Wang, *Nano Lett.*, 2010, **10**, 799–803.
13 P. Pieranski, *Phys. Rev. Lett.*, 1980, **45**, 569–572.
14 Y. Xia, B. Gates, Y. Yin and Y. Lu, *Adv. Mater.*, 2000, **12**, 693–713.
15 J. Aizenberg, P. V. Braun and P. Wiltzius, *Phys. Rev. Lett.*, 2000, **84**, 2997–3000.
16 M. Sastry, M. Rao and K. N. Ganesh, *Acc. Chem. Res.*, 2002, **35**, 847–855.
17 K. A. Taylor and D. W. Taylor, *J. Mol. Biol.*, 1993, **230**, 196–205.
18 S. A. Darst, H. O. Ribi, D. W. Pierce and R. D. Kornberg, *J. Mol. Biol.*, 1988, **203**, 269–273.
19 S. S. Stoylova, P. J. Lenting, G. Kemball-Cook and A. Holzenburg, *J. Biol. Chem.*, 1999, **274**, 36573–36578.
20 L. Ramos, T. C. Lubensky, N. Dan, P. Nelson and D. A. Weitz, *Science*, 1999, **286**, 2325–2328.
21 G. Kaur, J. B. He, J. Xu, S. V. Pingali, G. Jutz, A. Boker, Z. Niu, T. Li, D. Rawlinson, T. Emrick, B. Lee, P. Thiyagarajan, T. P. Russell and Q. Wang, *Langmuir*, 2009, **25**, 5168–5176.
22 L. Yang, S. T. Wang, M. Fukuto, A. Checco, Z. Niu and Q. Wang, *Soft Matter*, 2009, **5**, 4951–4961.
23 W. M. Gelbart, R. F. Bruinsma, P. A. Pincus and V. A. Parsegian, *Phys. Today*, 2000, **53**, 38–44.
24 J. Israelachvili, *Intermolecular and Surface Forces*, Academic, London, 1992.
25 K. Wagner, D. Harries, S. May, V. Kahl, J. O. Radler and A. Ben-Shaul, *Langmuir*, 2000, **16**, 303–306.
26 G. P. Lomonossoff and J. E. Johnson, *Prog. Biophys. Mol. Biol.*, 1991, **55**, 107–137.
27 T. Schmidt, J. E. Johnson and W. E. Phillips, *Virology*, 1983, **127**, 65–73.
28 T. W. Lin, Z. G. Chen, R. Usha, C. V. Stauffacher, J.-B. Dai, T. Schmidt and J. E. Johnson, *Virology*, 1999, **265**, 20–34.
29 R. Usha, J. E. Johnson, D. Moras, J. C. Thierry, R. Fourme and R. Kahn, *J. Appl. Crystallogr.*, 1984, **17**, 147–153.
30 J. M. White and J. E. Johnson, *Virology*, 1980, **101**, 319–324.
31 J. E. Johnson and C. Hollingshead, *J. Ultrastruct. Res.*, 1981, **74**, 223–231.
32 Y. Jia and X.-Y. Liu, *J. Phys. Chem. B*, 2006, **110**, 6949–6955.
33 K. Aoyama, K. Ogawa, Y. Kimura and Y. Fujiyoshi, *Ultramicroscopy*, 1995, **57**, 345–354.
34 M. Okuda, Y. Kobayashi, K. Suzuki, K. Sonoda, T. Kondoh, A. Wagawa, A. Kondo and H. Yoshimura, *Nano Lett.*, 2005, **5**, 991–993.
35 C. L. Cheung, A. I. Rubinstein, E. J. Peterson, A. Chatterji, R. F. Sabirianov, W. N. Mei, T. Lin, J. E. Johnson and J. J. DeYoreo, *Langmuir*, 2010, **26**, 3498–3505.
36 D. Baranov, A. Fiore, M. van Huis, C. Giannini, A. Falqui, U. Lafont, H. Zandbergen, M. Zanella, R. Cingolani and L. Manna, *Nano Lett.*, 2010, **10**, 743–749.
37 S. Srivastava, B. Samanta, B. J. Jordan, R. Hong, Q. Xiao, M. T. Tuominen and V. M. Rotello, *J. Am. Chem. Soc.*, 2007, **129**, 11776–11780.
38 A. George and W. W. Wilson, *Acta Crystallogr., Sect. D: Biol. Crystallogr.*, 1994, **50**, 361–365.
39 B. L. Neal, D. Asthagiri, O. D. Velev, A. M. Lenhoff and E. W. Kaler, *J. Cryst. Growth*, 1999, **196**, 377–387.
40 K. A. Kantardjieff and B. Rupp, *Bioinformatics*, 2004, **20**, 2162–2168.
41 Q. Wang, E. Kaltgrad, T. Lin, J. E. Johnson and M. G. Finn, *Chem. Biol.*, 2002, **9**, 805–811.
42 D. J. Siler, J. Babcock and G. Bruening, *Virology*, 1976, **71**, 560–567.
43 M. Fukuto, S. T. Wang, M. A. Lohr, S. Kewalramani and L. Yang, *Soft Matter*, 2010, **6**, 1513–1519.
44 L. K. Nielsen, T. Bjornholm and O. G. Mouritsen, *Langmuir*, 2007, **23**, 11684–11692.